

# Multiband optical flux and polarization variability of the blazar OJ 287 during 2016 – 2017

Alok C. Gupta<sup>1,2\*</sup>, Haritma Gaur<sup>2†</sup>, Paul J. Wiita<sup>3‡</sup>, A. Pandey<sup>1</sup>, P. Kushwaha<sup>4</sup>, S. M. Hu<sup>5</sup>, O. M. Kurtanidze<sup>6,7,8,9</sup>, E. Semkov<sup>10</sup>, G. Damljanovic<sup>11</sup>, A. Goyal<sup>12</sup>, M. Uemura<sup>13</sup>, A. Darriba<sup>14,15</sup>, Xu Chen<sup>5</sup>, O. Vince<sup>11</sup>, M. F. Gu<sup>2</sup>, Z. Zhang<sup>16</sup>, R. Bachev<sup>10</sup>, R. Itoh<sup>17</sup>, M. Kawabata<sup>13</sup>, S. O. Kurtanidze<sup>6</sup>, T. Nakaoka<sup>13</sup>, M. G. Nikolashvili<sup>6</sup>, L. A. Sigua<sup>6</sup>, L. Stawarz<sup>12</sup>, A. Strigachev<sup>10</sup>

<sup>1</sup>Aryabhatta Research Institute of Observational Sciences (ARIES), Manora Peak, Nainital – 263002, India

<sup>2</sup>Key Laboratory for Research in Galaxies and Cosmology, Shanghai Astronomical Observatory, Chinese Academy of Sciences, Shanghai 200030, China

<sup>3</sup>Department of Physics, The College of New Jersey, P.O. Box 7718, Ewing, NJ 08628-0718, USA

<sup>4</sup>Department of Astronomy (IAG-USP), University of São Paulo, São Paulo 05508-900, Brazil

<sup>5</sup>Shandong Provincial Key Laboratory of Optical Astronomy and Solar-Terrestrial Environment, Institute of Space Sciences, Shandong University, Weihai 264209, China

<sup>6</sup>Abastumani Observatory, Mt. Kanobili, 0301 Abastumani, Georgia

<sup>7</sup>Engelhardt Astronomical Observatory, Kazan Federal University, Tatarstan, Russia

<sup>8</sup>Center for Astrophysics, Guangzhou University, Guangzhou 510006, China

<sup>9</sup>Key Laboratory of Optical Astronomy, National Astronomical Observatories, Chinese Academy of Sciences, Beijing 100012, China

<sup>10</sup>Institute of Astronomy and National Astronomical Observatory, Bulgarian Academy of Sciences, 72 Tsarigradsko Shosse Blvd., 1784 Sofia, Bulgaria

<sup>11</sup>Astronomical Observatory, Volgina 7, 11060 Belgrade, Serbia

<sup>12</sup>Astronomical Observatory of Jagiellonian University, ul. Orla 171, 30-244 Krakw, Poland

<sup>13</sup>Hiroshima Astrophysical Science Center, Hiroshima University, Kagamiyama 1-3-1, Higashi-Hiroshima 739-8526, Japan

<sup>14</sup>American Association of Variable Star Observers (AAVSO), 49 Bay State Rd., Cambridge, MA 02138, USA

<sup>15</sup>Group M1, Centro Astronómico de Avila, Madrid, Spain

<sup>16</sup>Shanghai Astronomical Observatory, Key Laboratory of Radio Astronomy, Chinese Academy of Sciences, Shanghai 200030, China

<sup>17</sup>Department of Physics, Tokyo Institute of Technology, 2-12-1 Ookayama, Meguro-ku, Tokyo 152-8551, Japan

Accepted ... Received ...; in original form ...

## ABSTRACT

We report on our recent multi-band optical photometric and polarimetric observational campaign of the blazar OJ 287 which was carried out during September 2016 – December 2017. We employed nine telescopes in Bulgaria, China, Georgia, Japan, Serbia, Spain and the United States. We collected over 1800 photometric image frames in BVRI bands and over 100 polarimetric measurements over  $\sim 175$  nights. In 11 nights with many quasi-simultaneous multi-band (V, R, I) observations, we did not detect any genuine intraday variability in flux or colour. On longer timescales multiple flaring events were seen. Large changes in colour with respect to time and in a colour–magnitude diagram were seen, and while no systematic variability trend was noticed in colour with respect to time, the colour–magnitude diagram shows a bluer-when-brighter trend. Large changes in the degree of polarization, and substantial swings in the polarization angle were detected. The fractional Stokes parameters of the polarization showed a systematic trend with time in the beginning of these observations, followed by chaotic changes and then an apparently systematic variation at the end. The spectral index shows a systematic variation with time and V-band magnitude and optical spectral energy distributions in outburst states, an intermediate state, and a low flux state, all show evidence of a blue bump. We briefly discuss possible physical mechanisms that could explain the observed flux, colour, polarization, and spectral variability.

**Key words:** galaxies: active – BL Lacertae objects: general – quasars: individual – BL Lacertae objects: individual: OJ 287

## 1 INTRODUCTION

Blazars comprise a subclass of radio-loud active galactic nuclei in which one of the relativistic jets emanating from the super massive black hole (SMBH) of mass  $10^6 - 10^{10} M_\odot$  is pointed close to the observer (Woo & Urry 2002). This class is composed of BL Lac objects, which have featureless or very weak emission lines (equivalent widths,  $EW \leq 5\text{\AA}$ ) (Stocke et al. 1991; Marcha et al. 1996) and flat spectrum radio quasars (FSRQs) which have prominent emission lines (Blandford & Rees 1978; Ghisellini et al. 1997). Blazars show flux variations across the complete electromagnetic (EM) spectrum on all possible time scales, i.e. as short as a few minutes to as long as several years. They show variable polarization in radio to optical bands, and their emission across the EM spectrum is predominantly non-thermal. Their multi-wavelength (MW) spectral energy distribution (SED) is a double humped structure in which the low energy hump peaks somewhere in IR to soft X-rays and is due to synchrotron emission from non-thermal electrons in the jet while the high energy hump peaks in GeV to TeV energies and is probably due to inverse-Compton up-scattering of synchrotron (SSC, synchrotron self Compton) or external photons (EC, external Compton) by the relativistic electrons producing the synchrotron emission (Kirk, Rieger, & Mastichiadis 1998; Gaur et al. 2010).

In the age of multi-wavelength (MW) transient astronomy, blazars are among the best types of persistent, but highly variable sources for which simultaneous MW observations should be performed in order to understand their emission mechanism over the complete EM spectrum. Flux and polarization variations in the range of minutes to less than a day is commonly called as intraday variability (IDV; Wagner & Witzel 1995) or microvariability (Miller, Carini, & Goodrich 1989) or intranight variability (Goyal et al. 2012), while those with timescales from days to a few months is called short term variability (STV), and timescale of several months to years is known as long term variability (LTV; Gupta et al. 2004). There is a series of papers in which blazars' optical flux and polarization variability on diverse timescales are reported (e.g. Andruhov et al. 2003, 2011; Gu et al. 2006; Cellone et al. 2007; Gaur, Gupta, & Wiita 2012a; Gaur et al. 2012b,c, 2014, 2015; Gupta et al. 2008, 2012, 2016, 2017a,b; Larionov et al. 2016; Kushwaha et al. 2018a, and references therein).

The blazar OJ 287 has been observed in the optical bands since  $\sim 1890$ , and by using about a century long light curve (LC), (Sillanpää et al. 1988) noticed that it showed double peaked outbursts almost every 12 years. To explain them they proposed a binary black hole model and predicted the next outbursts would occur in 1994–1995. An extensive optical monitoring campaign known as OJ-94 was organized around the globe and the predicted double peaked outbursts were indeed detected in 1994–1995 separated by  $\sim 1.2$  years (e.g. Sillanpää et al. 1996a,b). In the next intense observing campaign on OJ 287 during 2005 – 2007, the double peaked outbursts were again detected, with the first one at the end of 2005 and the second at the end of 2007, separated by  $\sim 2$  years (Valtonen et al. 2009). For the most recent prediction of double peaked outbursts, the first outburst was detected in December 2015 while the second outburst still has to be detected (Valtonen et al. 2016; Gupta et al. 2017a) and is predicted for mid-2019 (Valtonen et al. 2016).

The most puzzling issues in the double peaked outbursts of OJ 287 are the timing of the detection of the second outburst and its strength. From the last three sets of outbursts detected since 1994,

‡ Email: wiitap@tcnj.edu

it is now clear that they are not exactly periodic. (Lehto & Valtonen 1996) analyzed the substructure of major outbursts of OJ 287, identified sharp flares and connected these with a model in which a secondary SMBH crosses the accretion disk of the primary SMBH during their mutual binary orbit. They estimated the masses of the primary and secondary SMBHs to be  $17 \times 10^9 M_{\odot}$  and  $10^8 M_{\odot}$ , respectively. The original model of (Sillanpää et al. 1988) has been modified in different ways over the past decade. Valtonen et al. (2008a) claimed that the changing binary system provides evidence for the loss of orbital energy ( $\sim 10\%$ ) with the emission of gravitational waves from the system. Valtonen et al. (2008a, 2010) explain the deviations of the outbursts from strict periodicity as arising from this gravitational wave driven in spiraling of the binary black hole system present at the centre of OJ 287.

The recently detected December 2015 optical outburst was the brightest in the last three decades and showed a polarization of  $< 11\%$  (Valtonen et al. 2016; Gupta et al. 2017a; Kushwaha et al. 2018a). It also shows a clear signature of thermal emission (Valtonen et al. 2016; Kushwaha et al. 2018a). Using data from the last three outbursts detected since 1994, the masses of the primary and secondary black holes are estimated to be  $(1.83 \pm 0.01) \times 10^{10} M_{\odot}$  and  $(1.5 \pm 0.1) \times 10^8 M_{\odot}$ , respectively, and the spin of primary black hole is claimed to be  $0.313 \pm 0.01$  (Valtonen et al. 2016). A strong flare detected in March 2016 was comparably strong as the December 2015 outburst and had with similar polarization (Kushwaha et al. 2018a; Gupta et al. 2017a). In general, blazars, including OJ 287, evince large amplitude flares, so determining which of them are those outbursts that are actually caused by the impacts associated with the binary black hole model remains a problem. These outbursts are distinguished by comparatively low optical polarization (Valtonen et al. 2008b).

In the present work, we report detailed optical flux and polarization measurement taken during September 2016 – December 2017 of the blazar OJ 287. This is continuation of our ongoing optical monitoring campaign around the globe of OJ 287 since year 2015. In that earlier work we detected several flaring in flux and significant changes in the degree of polarization and polarization angle (Gupta et al. 2017a; Kushwaha et al. 2018a). We will continue our campaign on this blazar, at least until we see if we detect the second predicted outburst of the current pair in 2019.

We structured the paper as follows. In Section 2, we provide information about our new optical photometric and polarimetric observational data and its analysis. In Section 3, we present the results and we discuss them in Section 4. We summarize our results in Section 5.

## 2 OBSERVATIONS AND DATA REDUCTIONS

Our new optical photometric and polarimetric observational campaigns were carried out from September 2016 to December 2017. Photometric observations were carried out using nine telescopes located in Japan, China, Bulgaria (2 telescopes), Georgia, Serbia, Spain and USA (2 telescopes). Using these nine telescopes, photometric observations were taken on 174 observing nights during which we collected a total of 1829 image frames of OJ 287 in B, V, R, and I optical photometric bands. Optical polarimetric observations were done with two telescopes at Steward Observatory, USA. Polarimetric observations were carried out over 94 observing nights for which there were a total of 104 polarimetric measurements of OJ 287.

During our observing campaign, optical photometric and po-

larimetric observations of OJ 287 were performed by Steward Observatory, University of Arizona using the 2.3-m Bok and 1.54-m Kupier telescopes. We call these two telescopes collectively as telescope A in the photometric observation log provided in Table 1. The observations from them are taken from the public archive<sup>1</sup>. These photometric and polarimetric observations of OJ 287 were carried out using SPOL CCD Imaging/Spectropolarimeter attached to those two telescopes. Details about the instrument, observation and data analysis are provided in detail in Smith et al. (2009).

Observations from Weihai observatory of Shandong University employed the 1.0-m telescope at Weihai, China. This telescope is named as Telescope B in the observation log provided in Table 1. It is a classical Cassegrain telescope with a focal ratio of f/8. The telescope is equipped with a back-illuminated Andor DZ936 CCD camera and BVRI filters. We provide critical information about the telescope and CCD detector in Table 2 and additional details are given in Hu et al. (2014). Sky flats for each filter were taken at twilight, and usually 10 bias frames were taken at the beginning and the end of the observation. All frames were processed automatically by using an Interactive Data Language (IDL) procedure developed locally which is based on the NASA IDL astronomical libraries<sup>2</sup>. Firstly, all frames were bias and flat-field corrected. Secondly, the magnitude was derived by differential photometry technique using local standard stars 4, 10 and 11 in the blazar field (Fiorucci & Tosti 1996). The photometry radius was set to 14 pixels, and the inner and outer radius for sky brightness were set to 30 and 40 pixels, respectively. Most of our intensive observations targeting IDV were done using this telescope.

Our optical photometric observing campaign of the blazar OJ 287 in the B, V, R, and I passbands continued to use two telescopes in Bulgaria (0.7 m and 0.4 m) which are conflated as Telescope C in Table 1. These telescopes are equipped with CCD detectors and broad-band optical filters B, V, R, and I. Details of these telescopes and the CCDs mounted on telescopes C as well as details of the reduction procedures used are given in our earlier papers (Agarwal et al. 2015; Gupta et al. 2016).

Optical V band photometric observations of the blazar OJ 287 were carried out using a Celestron C14 XLT 35.6cm with reducer f/6.3 located at Las Casqueras, Spain. The telescope is equipped with CCD camera and V broad band optical filter and is called Telescope D in Table 1. Details about this telescope and CCD are given in Table 2. Standard image processing (bias, flat field and dark corrections) are applied and the photometry data were reduced using the Software MaxIm DL. Reference stars available in the database of the American Association of Variable Star Observers (AAVSO)<sup>3</sup> are used for calibrating the V magnitude of OJ 287.

For this campaign, observations of OJ 287 were also carried out using the newly installed 1.4-m telescope at ASV (Astronomical Station Vidojevica of the Astronomical Observatory in Belgrade). The telescope is equipped with CCD camera and B, V, R, I broad band optical Johnson-Cousins filters. Details are given in Table 2. During our observations, the CCD was cooled to 30°C below ambient. The camera is back-illuminated with high quantum efficiency (QE):peak QE at 550 nm  $> 90\%$ . The observations carried out by this telescope are given in the observation log reported in Table 1 where it is denoted as Telescope E. Photometric observations were done in  $1 \times 1$  binning mode in B, V, R, I pass-

<sup>1</sup> <http://james.as.arizona.edu/~psmith/Fermi/datause.html>

<sup>2</sup> <http://idlastro.gsfc.nasa.gov/>

<sup>3</sup> <https://www.aavso.org/apps/vsp/>

**Table 1.** Observation log of optical photometric observations of the blazar OJ 287.

Date yyyy mm dd	Telescope	Data Points B, V, R, I	Date yyyy mm dd	Telescope	Data Points B, V, R, I	Date yyyy mm dd	Telescope	Data Points B, V, R, I	Date yyyy mm dd	Telescope	Data Points B, V, R, I
2016 09 24	A	0, 1, 1, 0	2017 01 09	G	0, 1, 1, 0	2017 03 10	B	0, 1, 1, 1	2017 05 16	A	0, 1, 1, 0
2016 09 25	A	0, 1, 1, 0	2017 01 10	B	0, 1, 1, 1	2017 03 12	A	0, 1, 1, 0	2017 05 17	D	0, 1, 0, 0
2016 10 09	B	0, 1, 1, 1	2017 01 11	A	0, 1, 1, 0	2017 03 12	B	0, 1, 1, 1	2017 05 19	B	0, 1, 1, 1
2016 10 10	B	0, 1, 1, 1	2017 01 12	A	0, 1, 1, 0	2017 03 12	D	0, 1, 0, 0	2017 05 20	A	0, 1, 1, 0
2016 10 25	A	0, 1, 1, 0	2017 01 14	D	0, 1, 0, 0	2017 03 13	A	0, 1, 1, 0	2017 05 20	B	0, 1, 1, 1
2016 10 26	A	0, 1, 1, 0	2017 01 15	D	0, 1, 0, 0	2017 03 13	B	0, 1, 1, 1	2017 05 21	A	0, 1, 1, 0
2016 10 27	A	0, 1, 1, 0	2017 01 17	G	0, 1, 1, 0	2017 03 14	A	0, 1, 1, 0	2017 05 21	B	0, 1, 1, 1
2016 10 28	F	0, 0, 4, 0	2017 01 18	F	0, 0, 3, 0	2017 03 15	F	0, 0, 4, 0	2017 05 22	A	0, 1, 1, 0
2016 10 29	A	0, 2, 2, 0	2017 01 21	D	0, 1, 0, 0	2017 03 18	B	0, 4, 4, 4	2017 05 22	F	0, 0, 4, 0
2016 10 29	B	0, 1, 1, 1	2017 01 22	D	0, 1, 0, 0	2017 03 18	D	0, 1, 0, 0	2017 05 23	A	0, 1, 1, 0
2016 10 29	D	0, 1, 0, 0	2017 01 24	B	0, 1, 1, 1	2017 03 19	B	0,30,30,31	2017 05 24	A	0, 1, 1, 0
2016 10 30	A	0, 2, 2, 0	2017 01 26	G	0, 1, 0, 0	2017 03 19	D	0, 1, 0, 0	2017 05 24	B	0, 1, 1, 1
2016 11 03	B	0, 1, 1, 1	2017 01 27	A	0, 1, 1, 0	2017 03 20	B	0,20,21,21	2017 05 25	A	0, 1, 1, 0
2016 11 04	B	0, 1, 1, 1	2017 01 27	G	0, 1, 1, 0	2017 03 20	D	0, 1, 0, 0	2017 05 25	F	0, 0, 4, 0
2016 11 05	G	0, 1, 0, 0	2017 01 28	A	0, 1, 1, 0	2017 03 21	E	1,2, 2, 2	2017 06 08	F	0, 0, 4, 0
2016 11 08	B	0, 1, 1, 1	2017 01 29	A	0, 1, 1, 0	2017 03 25	D	0, 1, 0, 0	2017 06 11	A	0, 1, 1, 0
2016 11 11	F	0, 0, 2, 0	2017 01 29	C	6, 6, 6, 6	2017 03 27	B	0,14,14,14	2017 06 12	A	0, 1, 1, 0
2016 11 14	F	0, 0, 5, 0	2017 01 30	A	0, 1, 1, 0	2017 03 28	A	0, 1, 1, 0	2017 06 12	D	0, 1, 0, 0
2016 11 15	B	0, 1, 1, 1	2017 01 31	A	0, 1, 1, 0	2017 03 28	B	0, 2, 3, 3	2017 06 13	A	0, 1, 1, 0
2016 11 16	B	0, 1, 1, 1	2017 02 01	A	0, 1, 1, 0	2017 03 29	A	0, 1, 1, 0	2017 06 14	A	0, 1, 1, 0
2016 11 16	G	0, 1, 1, 0	2017 02 01	C	4, 4, 4, 4	2017 03 29	B	0, 5, 5, 5	2017 06 15	A	0, 1, 1, 0
2016 11 22	F	0, 0, 4, 0	2017 02 02	C	4, 4, 4, 4	2017 03 29	F	0, 0, 4, 0	2017 09 20	A	0, 1, 1, 0
2016 11 25	A	0, 1, 1, 0	2017 02 03	C	8, 8, 8, 8	2017 03 30	A	0, 1, 1, 0	2017 09 21	A	0, 1, 1, 0
2016 11 26	B	0, 1, 1, 1	2017 02 03	F	0, 0, 3, 0	2017 04 01	D	0, 1, 0, 0	2017 09 23	D	0, 1, 0, 0
2016 11 26	F	0, 0, 4, 0	2017 02 05	B	0, 1, 1, 1	2017 04 02	B	0,22,23,23	2017 09 25	D	0, 1, 0, 0
2016 11 27	B	0, 1, 1, 1	2017 02 11	G	0, 1, 1, 0	2017 04 03	B	0,21,22,23	2017 09 28	D	0, 1, 0, 0
2016 11 28	B	0, 1, 1, 1	2017 02 14	F	0, 0, 5, 0	2017 04 03	C	2, 5, 5, 2	2017 09 30	D	0, 1, 0, 0
2016 11 28	F	0, 0, 4, 0	2017 02 17	C	1, 3, 3, 1	2017 04 03	D	0, 1, 0, 0	2017 10 05	F	0, 0, 4, 0
2016 11 30	A	0, 1, 1, 0	2017 02 18	C	1, 4, 4, 1	2017 04 03	F	0, 0, 5, 0	2017 10 07	D	0, 1, 0, 0
2016 11 30	B	0, 1, 1, 1	2017 02 18	D	0, 1, 0, 0	2017 04 04	C	2, 4, 5, 2	2017 10 09	F	0, 0, 5, 0
2016 12 01	A	0, 1, 1, 0	2017 02 19	B	0, 1, 1, 1	2017 04 09	D	0, 1, 0, 0	2017 10 12	D	0, 1, 0, 0
2016 12 01	B	0, 1, 1, 1	2017 02 19	D	0, 1, 0, 0	2017 04 10	D	0, 1, 0, 0	2017 10 15	A	0, 1, 1, 0
2016 12 02	A	0, 1, 1, 0	2017 02 20	B	0,72,74,74	2017 04 12	F	0, 0, 2, 0	2017 10 16	A	0, 1, 1, 0
2016 12 02	B	0, 1, 1, 1	2017 02 20	F	0, 0, 4, 0	2017 04 14	B	0,13,13,13	2017 10 17	A	0, 1, 1, 0
2016 12 03	D	0, 1, 0, 0	2017 02 22	E	1, 1, 1, 1	2017 04 16	F	0, 0, 6, 0	2017 10 20	A	0, 1, 1, 0
2016 12 05	B	0, 1, 1, 1	2017 02 23	E	1, 1, 1, 1	2017 04 21	E	2, 2, 2, 2	2017 10 21	A	0, 1, 1, 0
2016 12 06	B	0, 1, 1, 1	2017 02 25	A	0, 1, 1, 0	2017 04 22	B	0, 1, 1, 1	2017 10 22	A	0, 1, 1, 0
2016 12 07	B	0, 1, 1, 1	2017 02 25	B	0,42,42,42	2017 04 23	D	0, 1, 0, 0	2017 10 22	D	0, 1, 0, 0
2016 12 07	F	0, 0, 4, 0	2017 02 25	D	0, 1, 0, 0	2017 04 24	D	0, 1, 0, 0	2017 10 24	F	0, 0, 4, 0
2016 12 09	F	0, 0, 4, 0	2017 02 26	B	0,40,40,40	2017 04 24	E	1, 1, 1, 1	2017 10 28	D	0, 1, 0, 0
2016 12 10	D	0, 1, 0, 0	2017 02 26	D	0, 1, 0, 0	2017 04 24	F	0, 0, 4, 0	2017 10 28	F	0, 0, 4, 0
2016 12 11	D	0, 1, 0, 0	2017 02 26	E	1, 1, 1, 1	2017 04 26	E	2, 2, 2, 2	2017 10 29	D	0, 1, 0, 0
2016 12 18	B	0, 1, 1, 1	2017 02 26	G	0, 1, 1, 0	2017 04 27	B	0, 1, 1, 1	2017 11 12	F	0, 0, 4, 0
2016 12 21	F	0, 0, 4, 0	2017 02 27	A	0, 1, 1, 0	2017 04 27	F	0, 0, 4, 0	2017 11 16	A	0, 1, 1, 0
2016 12 23	B	0, 1, 1, 0	2017 02 27	E	1, 1, 1, 1	2017 04 28	A	0, 1, 1, 0	2017 11 17	A	0, 1, 1, 0
2016 12 24	B	0, 1, 1, 0	2017 02 28	E	1, 1, 1, 1	2017 04 28	B	0, 1, 1, 1	2017 11 18	A	0, 1, 1, 0
2016 12 24	F	0, 0, 4, 0	2017 02 28	F	0, 0, 4, 0	2017 04 29	A	0, 1, 1, 0	2017 11 18	D	0, 1, 0, 0
2016 12 27	A	0, 1, 1, 0	2017 03 01	A	0, 1, 1, 0	2017 04 30	A	0, 1, 1, 0	2017 11 19	A	0, 1, 1, 0
2016 12 27	B	0, 1, 1, 1	2017 03 01	C	2, 4, 4, 1	2017 04 30	D	0, 1, 0, 0	2017 11 19	D	0, 1, 0, 0
2016 12 29	D	0, 2, 0, 0	2017 03 02	A	0, 1, 1, 0	2017 04 30	F	0, 0, 4, 0	2017 11 20	A	0, 1, 1, 0
2016 12 30	D	0, 2, 0, 0	2017 03 02	B	0,40,40,40	2017 05 01	A	0, 1, 1, 0	2017 11 22	A	0, 1, 1, 0
2016 12 31	D	0, 3, 0, 0	2017 03 02	E	1, 1, 1, 1	2017 05 01	B	0, 1, 1, 1	2017 12 08	A	0, 1, 1, 0
2017 01 03	A	0, 1, 1, 0	2017 03 03	E	1, 1, 1, 1	2017 05 02	A	0, 1, 2, 0	2017 12 09	A	0, 1, 1, 0
2017 01 03	C	2, 2, 1, 2	2017 03 03	F	0, 0, 3, 0	2017 05 02	B	0, 1, 2, 2	2017 12 09	D	0, 1, 0, 0
2017 01 03	F	0, 0, 4, 0	2017 03 05	B	0,42,42,42	2017 05 02	D	0, 1, 0, 0	2017 12 11	F	0, 0, 4, 0
2017 01 03	G	0, 1, 1, 0	2017 03 06	C	1, 5, 5, 2	2017 05 04	B	0, 1, 1, 1	2017 12 13	A	0, 1, 1, 0
2017 01 04	A	0, 1, 1, 0	2017 03 06	F	0, 0, 4, 0	2017 05 04	D	0, 1, 0, 0	2017 12 14	A	0, 1, 1, 0
2017 01 05	A	0, 1, 1, 0	2017 03 06	G	0, 1, 1, 0	2017 05 08	F	0, 0, 4, 0	2017 12 15	A	0, 1, 1, 0
2017 01 07	D	0, 1, 0, 0	2017 03 08	B	0, 1, 1, 1	2017 05 12	F	0, 0, 3, 0	2017 12 16	A	0, 1, 1, 0
2017 01 07	F	0, 0, 4, 0	2017 03 09	A	0, 1, 1, 0	2017 05 14	A	0, 1, 1, 0	2017 12 16	D	0, 1, 0, 0
2017 01 08	D	0, 1, 0, 0	2017 03 09	G	0, 1, 1, 0	2017 05 14	B	0, 1, 1, 1	2017 12 17	D	0, 1, 0, 0
2017 01 09	F	0, 0, 4, 0	2017 03 10	A	0, 1, 1, 0	2017 05 15	A	0, 1, 1, 0			

A: 2.3-m Bok Telescope and 1.54-m Kuiper Telescope at Steward Observatory, Arizona, USA

B: 1.0-m Cassegrain Telescope in Weihai, China

C: 2-m Ritchey-Chretien Telescope and 50/70-cm Schmidt Telescope at National Astronomical Observatory, Rozhen, Bulgaria

D: 35.6 cm Telescope at Observatorio Astronómico Las Casqueras, Spain

E: 1.4-m Telescope, Astronomical Station Vidojevica (ASV), Serbia

F: 70-cm meniscus telescope at Abastumani Observatory, Georgia

G: 1.5-m KANATA telescope at HigashiHiroshima Observatory, Japan

bands. Standard optical photometric data analysis procedures were adopted (e.g. bias and flat field correction). To obtain instrumental B, V, R, I magnitudes of OJ 287 and comparison stars, usually we took 3 image frames per filter, and the result is the average value of the estimated magnitude. Local standard stars in the

blazar OJ 287 field are used to calibrate the magnitude of OJ 287 (Fiorucci & Tosti 1996).

Some data from the 70 cm telescope at Abastumani Observatory in Georgia were taken in R band and they are listed as Telescope F in the photometric observation log given in Table 1.

**Table 2.** Details of new telescopes and instruments

	Weihai, China	Las Casqueras, Spain	ASV, Serbia
Telescope	1.0-m Cassegrain	35.6 cm Schmidt Cassegrain	1.4-m RC Nasmyth
CCD Model	Andor DZ936	ATIK 383L+ Monochrome	Apogee Alta U42
Chip Size	2048 × 2048 pixels <sup>2</sup>	3354 × 2529 pixels <sup>2</sup>	2048 × 2048 pixels <sup>2</sup>
Scale	0.35 arc sec pixel <sup>-1</sup>	1.38 arc sec pixel <sup>-1</sup>	0.243 arc sec pixel <sup>-1</sup>
Field	12 × 12 arcmin <sup>2</sup>	25.46 × 19.16 arcmin <sup>2</sup>	8.3 × 8.3 arcmin <sup>2</sup>
Gain	1.8 e <sup>-1</sup> ADU <sup>-1</sup>	0.41 e <sup>-1</sup> ADU <sup>-1</sup>	1.25 e <sup>-1</sup> ADU <sup>-1</sup>
Read out noise	7 e <sup>-1</sup> rms	7 e <sup>-1</sup> rms	7 e <sup>-1</sup> rms
Typical Seeing	1.3 – 2 arcsec	1.5 – 2.5 arcsec	1 – 1.5 arcsec

The 1.5 m telescope in Kanata, Japan is named as Telescope G in that table and it also contributed data in V and R bands on a few nights. Details about telescopes F and G, their CCDs, broad band filters, and the data reduction employed are given in our earlier paper (Gupta et al. 2017a).

### 3 RESULTS

In Fig. 1 we present the photometric and polarimetric light curves (LCs) generated from our observing campaign using nine telescopes around the globe during September 2016 – December 2017. We present LCs of B mag, V mag, R mag, I mag, as well as the degree of polarization and polarization angle. The V and R band LCs clearly have the densest observational cadence. The polarimetric observations do not have similarly dense coverage as the most common photometric observations in the V and R bands. One can immediately notice that there are several flaring events in the photometric observations in V and R bands, as well as large changes in the degree of polarization and polarization angle. In the following subsections, we discuss the variability characteristics of the blazar OJ 287 on IDV, STV and LTV timescales, and the nature of the polarization variation.

#### 3.1 Light Curve Analysis Techniques

To quantify the variability results, we use variability detection techniques based on the *F*-Test and  $\chi^2$ -Test and we describe them briefly in the following subsections. We claim a LC is variable only if the variability is detected by both the tests. We also calculate the variability amplitude on IDV and LTV timescales. The method used to determine the variability amplitude is also described briefly below.

##### 3.1.1 *F*-Test

To quantify any IDV of the blazar OJ 287, we adopted the commonly used *F*-Test (de Diego 2010). We employ two comparison stars and so define (Gaur, Gupta, & Wiita 2012a; Agarwal & Gupta 2015; Gupta et al. 2017a, and the references therein),

$$F_1 = \frac{\text{Var}(\text{BL} - \text{star1})}{\text{Var}(\text{star1} - \text{star2})}, F_2 = \frac{\text{Var}(\text{BL} - \text{star1})}{\text{Var}(\text{star1} - \text{star2})} \quad (1)$$

where (BL – star 1), (BL – star 2), and (star 1 – star 2) are the differential instrumental magnitudes of blazar and standard star 1, blazar and standard star 2, and standard star 1 and standard star 2, respectively, while  $\text{Var}(\text{BL} - \text{star1})$ ,  $\text{Var}(\text{BL} - \text{star2})$ , and  $\text{Var}(\text{star1} - \text{star2})$  are the variances of the differential instrumental magnitudes of blazar and standard star 1, blazar and standard star 2, and standard star 1 and standard star 2, respectively.

1 – star 2) are the variances of the differential instrumental magnitudes.

Then the relevant *F* value is the average of  $F_1$  and  $F_2$  which is then compared with the critical  $F_{\nu_{bl}, \nu_*}^{(\alpha)}$  value where  $\alpha$  is the significance level set for the test while  $\nu_{bl}$  and  $\nu_*$  are the number of degrees of freedom, calculated as  $(N - 1)$ , with  $N$  the number of measurements. For IDV detection in the LCs, we have done the *F*-test for  $\alpha$  values of 0.999 and 0.99, which effectively correspond to  $3\sigma$  and  $2.6\sigma$  detections, respectively. The null hypothesis (no variability) is discarded if the *F* value is greater than the critical value, and as usual we claim a LC to be variable if  $F > F_c(0.99)$  (Agarwal & Gupta 2015; Gupta et al. 2017a).

##### 3.1.2 $\chi^2$ -Test

To quantify the detection of variability of the blazar we have also used the  $\chi^2$ -Test (de Diego 2010). The  $\chi^2$  statistic is defined as (e.g. Agarwal & Gupta 2015)

$$\chi^2 = \sum_{i=1}^N \frac{(V_i - \bar{V})^2}{\sigma_i^2}, \quad (2)$$

where,  $\bar{V}$  is the average magnitude, and  $V_i$  is the magnitude of  $i^{th}$  observation with a corresponding standard error  $\sigma_i$ . It has been determined that the actual measurement errors are larger than the errors indicated by photometry software by a factor of 1.3 – 1.75 (e.g. Gopal-Krishna et al. 2003). So we multiply the errors obtained from the data reductions by a factor of 1.5 (Stalin et al. 2004) to get better estimates of the real photometric errors. The mean value of  $\chi^2$  is then compared with the critical value  $\chi_{\alpha, \nu}^2$  where  $\alpha$  is the significance level and  $\nu = N - 1$  is the number of degrees of freedom. A value  $\chi^2 > \chi_{\alpha, \nu}^2$  implies the presence of variability.

We list a source as Variable (Var) only if it satisfies both the *F*-test and the  $\chi^2$ -Test for  $\alpha = 0.99$ .

##### 3.1.3 Amplitude of Variability

The percentage of magnitude and colour variations on IDV through LTV time scales can be calculated by using the variability amplitude parameter  $A$ , which was introduced by Heidt & Wagner (1996) and defined as

$$A = 100 \times \sqrt{(A_{\text{max}} - A_{\text{min}})^2 - 2\sigma^2} (\%) \quad (3)$$

Here  $A_{\text{max}}$  and  $A_{\text{min}}$  are the maximum and minimum values in the calibrated magnitude and colour of LCs of the blazar, and  $\sigma$  is the average measurement error.

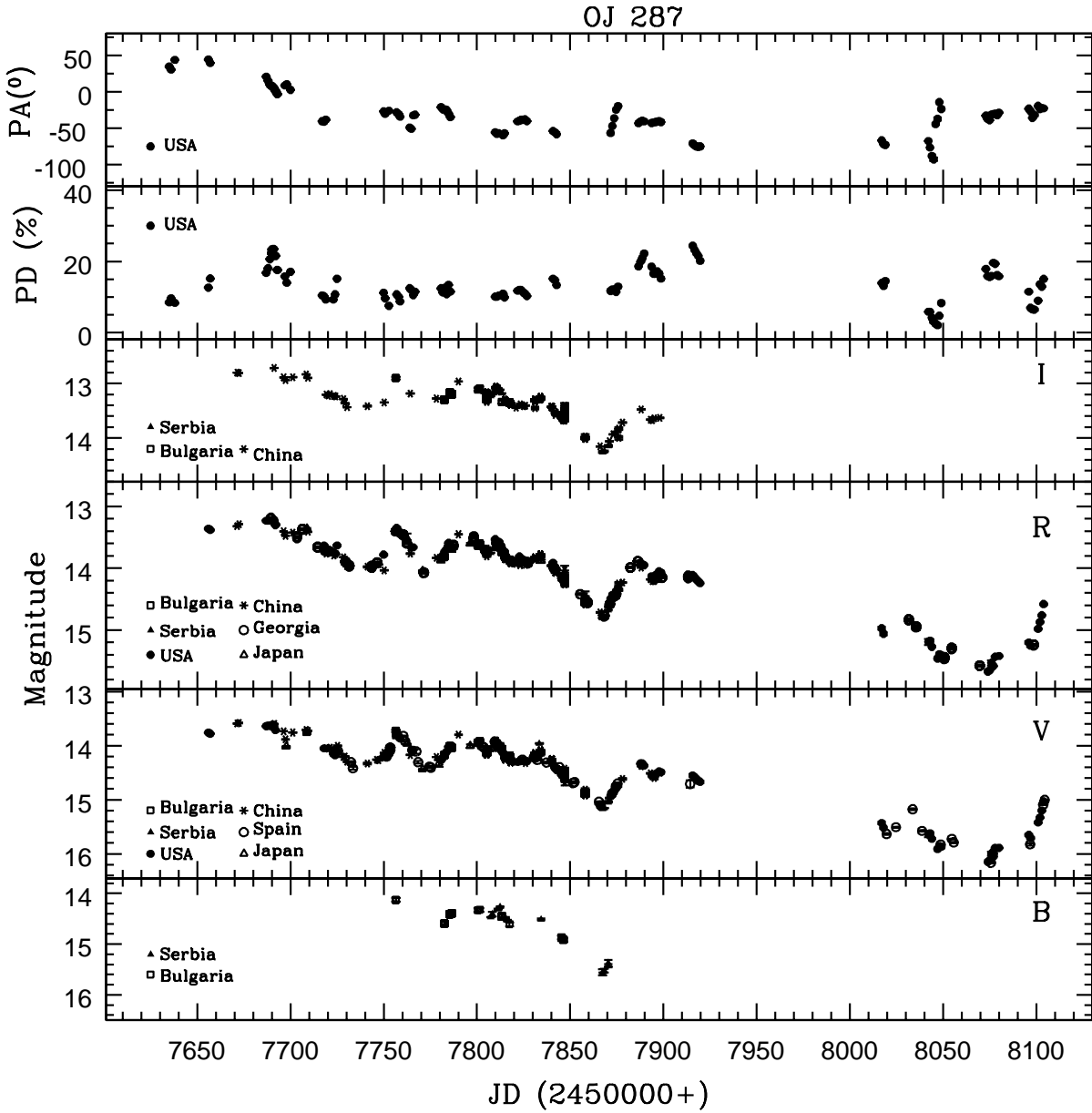


**Figure 1.** Optical flux and polarization variability light curves of OJ 287 during September 2015 – December 2017. From bottom to top, the panels show B magnitude, V magnitude, R magnitude, I magnitude, degree of polarization in R band, and polarization angle in R band, respectively. Different symbols marked inside the panels represent the data from different telescopes.

### 3.2 Intra-day Flux and Colour Variability

Out of  $\sim 175$  observing nights during the campaign, we have many nights when multiple image frames were observed in any specific optical band. But to study the optical flux and colour variability properties on IDV timescales, we selected only nights with a minimum of ten observations in an optical band by a telescope on a particular observing night, and for plotting the IDV LCs, we decided on a minimum of twenty observations in an optical band by a telescope on a particular observing night. Using this criteria, eleven observing nights qualified for IDV flux and colour variability analysis and the results are reported in Table 3, while nine multi-band optical IDV flux LCs are plotted in Fig. 2.

To investigate the flux and colour variability on IDV timescales on the above nights, we have used  $F$ -Test and  $\chi^2$ -Test

analyses which were briefly explained in section 3.1.1 and 3.1.2, respectively. Using these tests, the presence or absence of IDV are reported in Table 3 where NV, PV and Var represent non-variable, possible variable and variable natures of LC. It is clearly seen from the plots in Fig. 2 as well as the results reported in Table 3 that, perhaps surprisingly, no genuine IDV was detected in any of the V, R, and I bands IDV LCs in the eight nights of intensive observations that were taken during 20 February 2017 – 2 April 2017. Given the lack of variability in any bands, it is obvious that no colour variations were seen on any of these nights on IDV timescales. But on 3 April 2017 there is hint of IDV detection in I band magnitude and R-I colour. On visual inspection we noticed that toward the end of that observation, the data is noisier and have large scatter, so, we only claim it as PV. However, it should be noted that nearly all of

**Table 3.** Results of IDV Observations. In the Variable column, Var, NV and PV represent variable, non-variable, and possible variable, respectively.

Date yyyymmdd	Band	N	F-test		$\chi^2$ -test		Variable	A (percent)
			$F_1, F_2, F, F_c(0.99), F_c(0.999)$		$\chi^2_1, \chi^2_2, \chi^2_{av}, \chi^2_{0.99}, \chi^2_{0.999}$			
20170220	V	74	0.98, 0.67, 0.83, 1.73, 2.08		75.73, 127.15, 101.44, 104.01, 116.09		NV	-
	R	74	1.50, 0.90, 1.20, 1.73, 2.08		59.06, 70.95, 65.00, 104.01, 116.09		NV	-
	I	74	1.18, 0.22, 0.70, 1.73, 2.08		320.75, 102.60, 211.67, 104.01, 116.09		NV	-
	(V-R)	74	1.00, 0.61, 0.81, 1.73, 2.08		75.76, 94.15, 84.96, 104.01, 116.09		NV	-
	(R-I)	74	1.28, 0.32, 0.80, 1.73, 2.08		209.11, 91.13, 150.12, 104.01, 116.09		NV	-
20170225	V	42	1.33, 1.07, 1.20, 2.09, 2.69		64.38, 89.91, 77.14, 64.95, 74.74		NV	-
	R	42	0.99, 0.57, 0.78, 2.09, 2.69		45.44, 54.48, 49.96, 64.95, 74.74		NV	-
	I	42	1.25, 0.45, 0.85, 2.09, 2.69		69.55, 69.87, 69.71, 64.95, 74.74		NV	-
	(V-R)	42	1.11, 0.67, 0.89, 2.09, 2.69		58.40, 65.31, 61.86, 64.95, 74.74		NV	-
	(R-I)	42	0.86, 0.36, 0.61, 2.09, 2.69		42.22, 40.86, 41.54, 64.95, 74.74		NV	-
20170226	V	40	0.75, 0.59, 0.67, 2.14, 2.76		28.52, 37.43, 32.98, 62.43, 72.05		NV	-
	R	40	1.34, 0.41, 0.87, 2.14, 2.76		42.34, 25.48, 33.91, 62.43, 72.05		NV	-
	I	40	1.63, 1.71, 1.67, 2.14, 2.76		99.83, 297.21, 198.52, 62.43, 72.05		NV	-
	(V-R)	40	0.92, 0.47, 0.69, 2.14, 2.76		31.11, 29.89, 30.50, 62.43, 72.05		NV	-
	(R-I)	40	1.28, 1.07, 1.17, 2.14, 2.76		42.85, 89.63, 66.24, 62.43, 72.05		NV	-
20170302	V	40	0.01, 1.00, 0.50, 2.14, 2.76		36.60, 16199.26, 8117.93, 62.43, 72.05		NV	-
	R	40	0.82, 0.65, 0.73, 2.14, 2.76		33.40, 47.76, 40.58, 62.43, 72.05		NV	-
	I	40	0.81, 0.52, 0.66, 2.14, 2.76		45.41, 72.59, 59.00, 62.43, 72.05		NV	-
	(V-R)	40	0.01, 1.01, 0.51, 2.14, 2.76		31.13, 10152.35, 5091.74, 62.43, 72.05		NV	-
	(R-I)	40	0.67, 0.34, 0.50, 2.14, 2.76		30.29, 31.23, 30.76, 62.43, 72.05		NV	-
20170305	V	42	0.82, 1.25, 1.04, 2.09, 2.69		94.44, 180.37, 137.40, 64.95, 74.74		NV	-
	R	42	1.07, 0.76, 0.91, 2.09, 2.69		41.57, 52.40, 46.99, 64.95, 74.74		NV	-
	I	42	0.95, 1.53, 1.24, 2.09, 2.69		45.93, 173.14, 109.53, 64.95, 74.74		NV	-
	(V-R)	42	0.70, 1.06, 0.88, 2.09, 2.69		69.68, 140.25, 104.96, 64.95, 74.74		NV	-
	(R-I)	42	1.80, 1.37, 1.59, 2.09, 2.69		33.84, 52.25, 43.04, 64.95, 74.74		NV	-
20170318	V	34	1.04, 0.49, 0.77, 2.29, 3.04		69.45, 50.13, 59.79, 54.78, 63.87		NV	-
	R	34	0.91, 0.23, 0.57, 2.29, 3.04		31.47, 19.34, 25.41, 54.78, 63.87		NV	-
	I	34	1.13, 0.35, 0.74, 2.29, 3.04		86.52, 85.94, 86.23, 54.78, 63.87		NV	-
	(V-R)	34	1.07, 0.40, 0.73, 2.29, 3.04		54.81, 35.10, 44.95, 54.78, 63.87		NV	-
	(R-I)	34	1.34, 0.35, 0.84, 2.29, 3.04		60.30, 41.54, 50.92, 54.78, 63.87		NV	-
20170321	V	20	1.89, 1.30, 1.59, 3.03, 4.47		25.04, 26.99, 26.01, 36.19, 43.82		NV	-
	R	20	2.18, 1.61, 1.89, 3.03, 4.47		37.44, 44.85, 41.15, 36.19, 43.82		NV	-
	I	20	1.39, 2.76, 2.07, 3.03, 4.47		45.26, 237.09, 141.18, 36.19, 43.82		NV	-
	(V-R)	20	1.55, 1.54, 1.55, 3.03, 4.47		13.05, 22.34, 17.69, 36.19, 43.82		NV	-
	(R-I)	20	0.52, 0.68, 0.60, 3.03, 4.47		13.16, 32.16, 22.66, 36.19, 43.82		NV	-
20170327	V	14	1.25, 1.36, 1.30, 3.91, 6.41		10.34, 17.36, 13.85, 27.69, 34.53		NV	-
	R	14	1.13, 0.38, 0.75, 3.91, 6.41		12.31, 6.75, 9.53, 27.69, 34.53		NV	-
	I	14	0.66, 0.15, 0.40, 3.91, 6.41		30.86, 17.90, 24.38, 27.69, 34.53		NV	-
	(V-R)	14	1.16, 0.75, 0.96, 3.91, 6.41		12.68, 13.10, 12.89, 27.69, 34.53		NV	-
	(R-I)	14	0.79, 0.19, 0.49, 3.91, 6.41		25.26, 12.96, 19.11, 27.69, 34.53		NV	-
20170402	V	22	1.16, 0.67, 0.91, 2.86, 4.13		45.23, 32.01, 38.62, 38.93, 46.80		NV	-
	R	22	0.58, 0.69, 0.64, 2.86, 4.13		12.55, 20.44, 16.49, 38.93, 46.80		NV	-
	I	22	0.92, 1.77, 1.35, 2.86, 4.13		32.55, 127.83, 80.19, 38.93, 46.80		NV	-
	(V-R)	22	1.17, 0.52, 0.84, 2.86, 4.13		40.16, 19.89, 30.03, 38.93, 46.80		NV	-
	(R-I)	22	0.76, 1.12, 0.94, 2.86, 4.13		27.05, 52.58, 39.82, 38.93, 46.80		NV	-
20170403	V	23	1.37, 0.65, 1.01, 2.78, 3.98		33.08, 22.98, 28.03, 40.29, 48.27		NV	-
	R	23	1.74, 0.49, 1.12, 2.78, 3.98		18.18, 14.12, 16.15, 40.29, 48.27		NV	-
	I	23	10.81, 6.47, 8.64, 2.78, 3.98		140.42, 126.98, 133.70, 40.29, 48.27		PV	27.3
	(V-R)	23	1.47, 0.62, 1.04, 2.78, 3.98		23.58, 21.17, 22.37, 40.29, 48.27		NV	-
	(R-I)	23	6.27, 3.07, 4.67, 2.78, 3.98		73.68, 60.45, 67.06, 40.29, 48.27		PV	25.2
20170414	V	13	3.46, 2.00, 2.73, 4.16, 7.00		7.22, 5.25, 6.23, 26.22, 32.91		NV	-
	R	13	0.36, 1.36, 0.86, 4.16, 7.00		10.37, 15.92, 13.14, 26.22, 32.91		NV	-
	I	13	3.92, 2.29, 3.10, 4.16, 7.00		31.81, 15.01, 23.41, 26.22, 32.91		NV	-
	(V-R)	13	1.04, 1.56, 1.30, 4.16, 7.00		9.82, 10.66, 10.24, 26.22, 32.91		NV	-
	(R-I)	13	1.02, 0.19, 0.61, 4.16, 7.00		23.58, 7.70, 15.64, 26.22, 32.91		NV	-

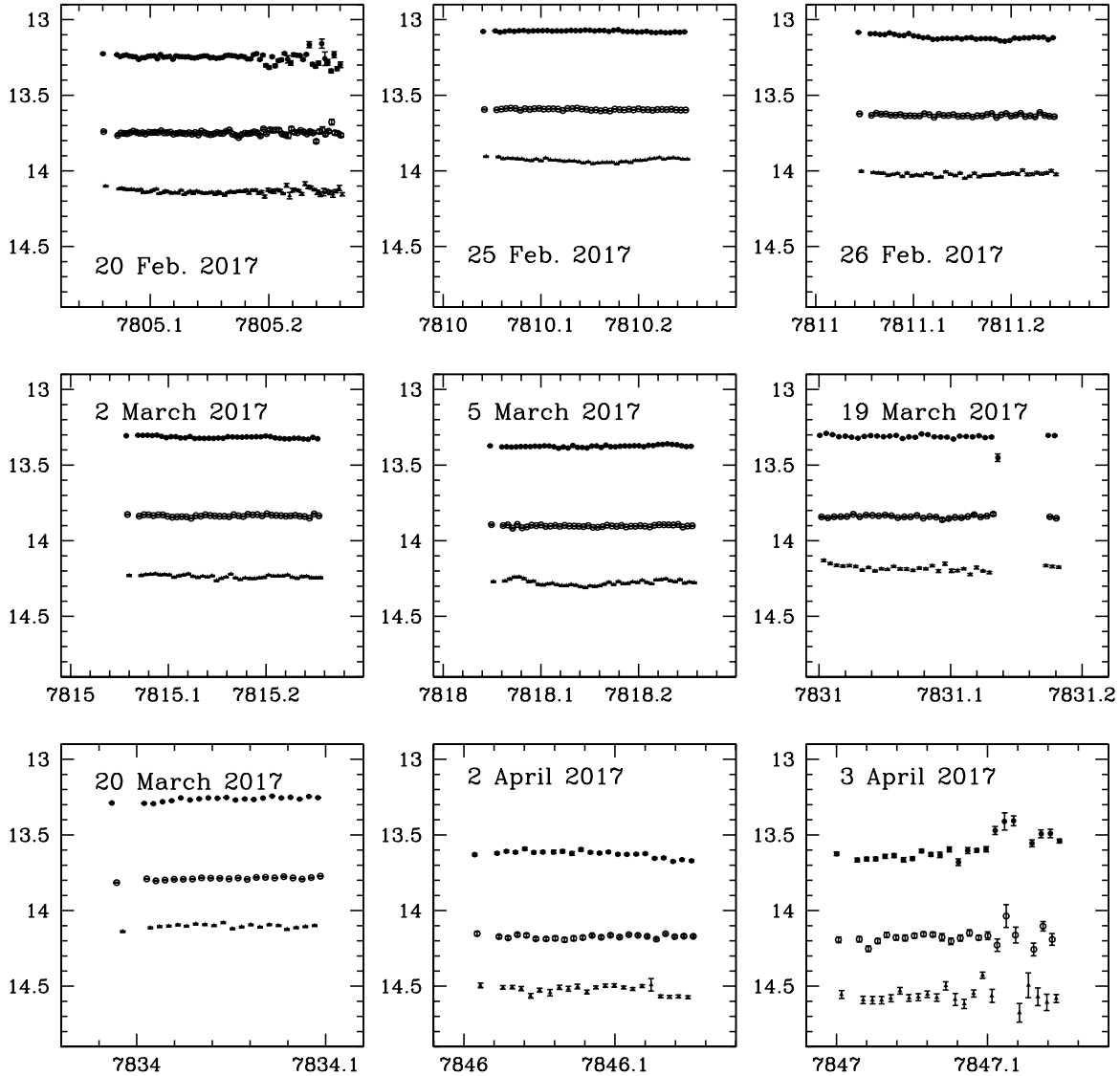


**Figure 2.** Intraday light curves for OJ 287 in V, R, I filters. Filled triangles, open circles and filled circles represent data in V, R, and I filters, respectively. The X axis is JD and the Y axis is the magnitude in each plot, where observation dates are indicated in each plot.

these nightly observations were relatively short, spanning between  $\sim 2.5$  and  $\sim 4$  hours, and so the chances of detecting IDV were limited.

From the LCs plotted in Figs. 1 and 2, it is can be seen that the blazar OJ 287 was in a fairly bright state during much of these observations. The brightest state detected in the blazar in the outburst in December 2015 was  $\sim 13.4$  mag in V, 13.0 mag in R, and 12.4 mag in I band (Gupta et al. 2017a). Just from these IDV LCs, we detected OJ 287 in the brightest state on 25 February 2017 when the magnitudes were  $\sim 13.9$  mag in V,  $\sim 13.6$  mag in R, and  $\sim 13.0$  mag in I bands.

### 3.3 Short and Long Term Variability

#### 3.3.1 Flux Variability

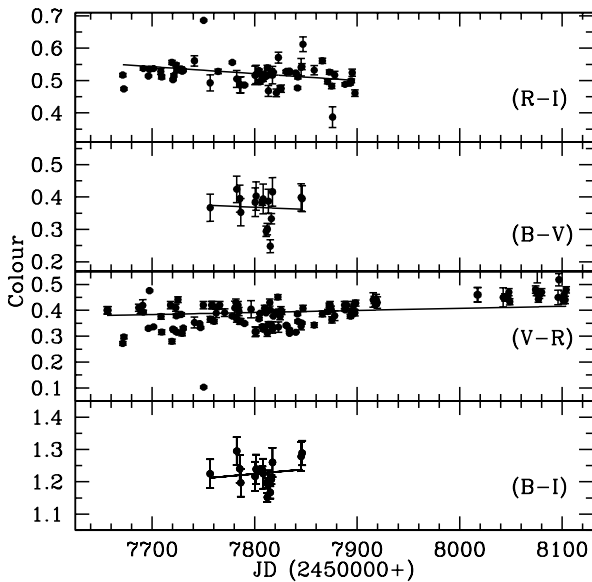
Significant flux variability of OJ 287 on STV and LTV timescales is evident from the four lower panels of Fig. 1 where the B, V, R, and

I band LCs are shown. We have calculated the variability amplitude in B, V, R, and I optical bands and these results are reported in Table 4. Observations in the B band were only carried out using telescopes in Bulgaria and Serbia for a total of sixteen observing nights between 3 January to 3 April 2017, while we have dense observations carried out in V, R, and I bands. We noticed that the faintest level of the blazar in B, V, R, I, bands respectively were 14.921 mag at JD 2457846.39561, 16.164 mag at JD 2458075.58133, 15.670 mag at JD 2458073.96976, and 14.154 mag at JD 2457866.00547. Similarly, the brightest levels we observed of the blazar in the B, V, R, I, bands were 14.126 mag at JD 2457756.53125, 13.582 mag at JD 2457672.36782, 13.179 mag at JD 2457679.620, and 12.720 mag at JD 2457691.29261, respectively. The amplitudes of variation in B, V, R, I bands are 79.5%, 258.2%, 249.1%, 143.4%, respectively, but the smaller values for the B and I bands are explained by the relative paucity of data for them, as all colours are seen to vary together when data were taken for all of them.

**Table 4.** Results of STV and LTV flux variations.

Band	Duration yyyy mm dd – yyyy mm dd	Variable	A (percent)
B	2017 01 03 – 2017 04 26	Var	79.5
V	2016 09 24 – 2017 12 17	Var	258.2
R	2016 09 24 – 2017 12 16	Var	249.1
I	2016 10 09 – 2017 05 24	Var	143.4

Note: Var: Variable; NV: non-variable

**Figure 3.** Optical colour variability light curves covering the entire monitoring period of OJ 287.**Table 5.** Color variation with respect to time on short and long timescales.

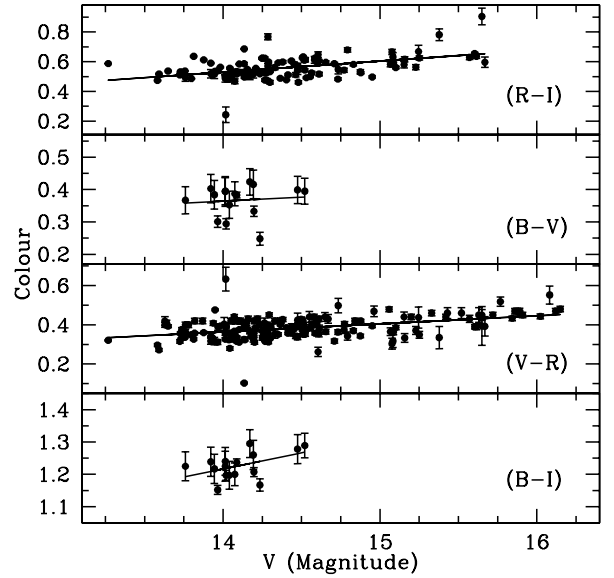
Color Indices	$m_1^a$	$c_1^a$	$r_1^a$	$p_1^a$
R-I	-2.147E-04	2.196	-0.567	2.771E-11
B-V	-1.293E-04	1.377	-0.059	0.830
V-R	7.981E-05	-0.231	0.307	4.106E-05
B-I	2.851E-04	-0.999	0.156	0.289

<sup>a</sup>  $m_1$  = slope and  $c_1$  = intercept of CI against JD;

$r_1$  = Pearson coefficient;  $p_1$  = null hypothesis probability

### 3.3.2 Color Variability

Optical colour variations with respect to time (colour vs time) and with respect to V band magnitude (colour vs magnitude) are plotted in Fig. 3 and Fig. 4, respectively. On visual inspection both the figures show clear colour variations. However, it seems there are no systematic trends in the colour variations, as shown by straight line fits to the colour vs time plot in Fig. 3. However, the colour vs magnitude plots in Fig. 4 show bluer-when-brighter (BWB) trends, which are significant for the more frequently measured V-R and R-I colours. Here lines,  $Y = mX + c$ , are fitted in to each panel

**Figure 4.** Optical colour-magnitude plots of OJ 287 during our entire monitoring period.

in Fig. 3 and Fig. 4. The values of the slopes,  $m$ , the intercepts,  $c$ , the linear Pearson correlation coefficients,  $r$ , and the corresponding null hypothesis probability,  $p$ , results for colour vs time and colour vs magnitude are reported in Table 5 and Table 6, respectively.

The extreme colour variations in Fig. 3 are the following: i) in R-I, 0.387 mag at JD 2457876.03118 and 0.686 mag at JD 2457750.21320 which show the change in colour is 0.299 mag; ii) in B-V, 0.248 mag at JD 2457815.22942 and 0.424 mag at JD 2457782.56575 or a change in colour of 0.176 mag; iii) in V-R, 0.103 mag at JD 2457750.21519 and 0.552 mag at JD 2458075.78911 which show the change in colour is 0.449 mag; iv) in B-I, 1.152 mag at JD 2457812.36413 and 1.295 mag at JD 2457782.54505 where the change in colour is 0.143 mag. Similarly, in the colour vs magnitude plots given in Fig. 4, the extreme colour variations are the following: i) in R-I, 0.461 mag at  $V = 14.480$  mag and 0.686 mag at  $V = 14.135$  mag which indicate the change in colour is 0.225 mag. ii) in B-V, 0.248 mag at  $V = 14.235$  mag and 0.424 mag at  $V = 14.170$  mag where the change in colour is 0.176 mag; iii) in V-R, 0.103 mag at  $V = 14.135$  mag and 0.552 mag at  $V = 16.082$  mag which show the change in colour is 0.449 mag; iv) in B-I, 1.152 mag at  $V = 13.966$  mag and 1.295 mag at  $V = 14.170$  mag with a change in colour is 0.143 mag.

### 3.3.3 Polarization Variability

In Fig. 1 we plotted optical magnitudes of OJ 287 as well as degree of polarization and polarization angle. It is clear from visual inspection of the figure that the source has shown large variation in degree of polarization, polarization angle as well as overall flux. We noticed the following pattern of variation of flux, degree of polarization, and polarization angle: (i) at  $\sim$  JD 2457682 the flare peak at  $R = 12.957$  mag corresponds to a degree of polarization 20%, and polarization angle  $15^\circ$ ; (ii) at  $\sim$  JD 2457755 flare peak at  $R = 13.35$  is anti-correlated with degree of polarization only 9% and the

**Table 6.** Color-magnitude dependencies and colour-magnitude correlation coefficients on short and long timescales.

Color Indices	$m_2^a$	$c_2^a$	$r_2^a$	$p_2^a$
R-I	7.447E-02	-0.513	0.487	3.319E-08
B-V	2.446E-02	0.022	0.097	0.721
V-R	4.093E-02	-0.209	0.440	1.577E-09
B-I	9.934E-02	-0.174	0.477	0.061

<sup>a</sup>  $m_2$  = slope and  $c_2$  = intercept of CI against V;  
 $r_2$  = Pearson coefficient;  $p_2$  = null hypothesis probability

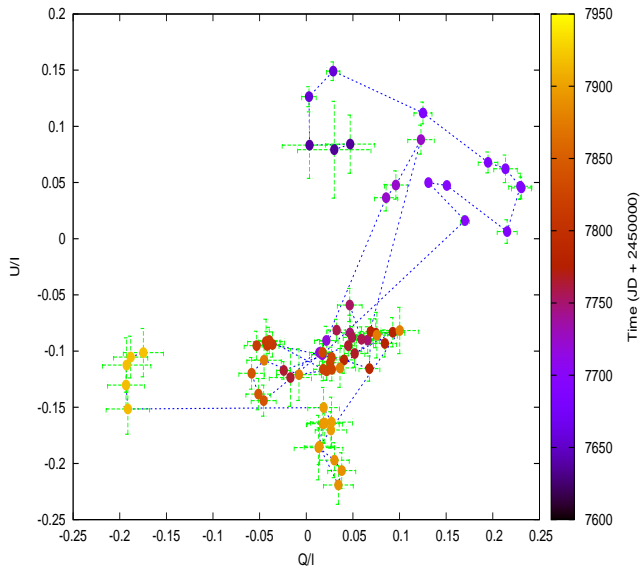


**Figure 5.** Fractional polarization variations over the course of data presented in this study.

polarization angle  $-35^\circ$ ; (iii) at  $\sim$  JD 2457790 the flare peak at  $R = 13.437$  mag corresponds to degree of polarization 13% and when the polarization angle  $-63^\circ$ ; (iv) at the lowest flux state at  $\sim$  JD 2458074 at  $R = 15.670$  mag is anti-correlated with a high degree of polarization,  $\sim 20\%$ , and the polarization angle  $-25^\circ$ .

Fig. 5 presents the polarization in terms of the normalized Stokes parameters, Q/I vs. U/I, for these data. Here we have used the data taken during  $\sim$  JD 2457633 to 2457920, before the  $\sim 100$  day gap when the blazar could not be observed from the ground. The more limited polarimetric observations taken afterwards have not been used in the analysis. We note there appears to be a systematic change in the polarization fluxes with the polarization angle during the first  $\sim 100$  days which evinces a clockwise loop-like structure (shown by black to purple points). During the middle part of the observations (red to yellow points) there is relatively less change in the Stokes parameters with roughly random variations. However, there is a hint of the beginning of a systematic change over the last 50 days of the observations (yellow points). Over all, the intensity variations in the Q,U-plane are mostly reminiscent of a random-walk indicating that emission is resulting from different regions with different magnetic field orientations (Moore et al. 1982), throughout the course of observations presented in this study.

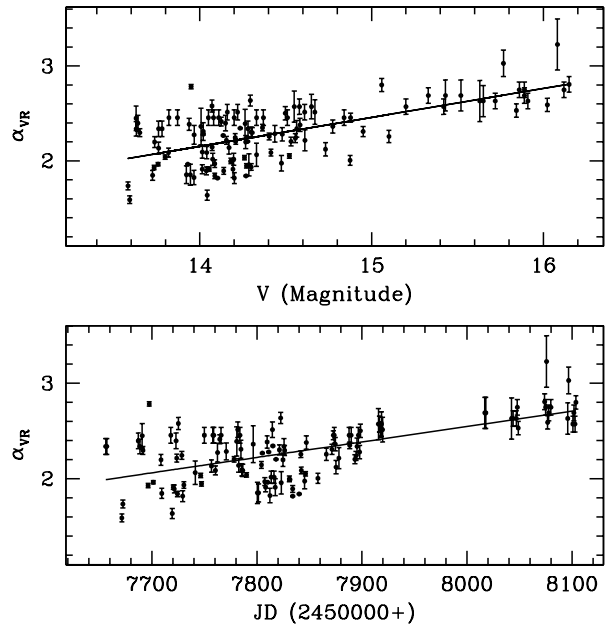


**Figure 6.** Optical spectral index variation with respect to time and V band magnitude covering the entire monitoring period of OJ 287.

### 3.3.4 Spectral Index Variation and Spectral Energy Distribution

We have dense sampling in V and R bands during our whole observing campaign, so, we also calculated spectral indices for all the epochs where we have V and R bands data on same JD using (Wierzcholska et al. 2015)

$$\langle \alpha_{VR} \rangle = \frac{0.4 \langle V - R \rangle}{\log(\nu_V / \nu_R)} \quad (4)$$

where  $\nu_V$  and  $\nu_R$  are effective frequencies of V and R bands, respectively (Bessell, Castelli, & Plez 1998). The spectral index with respect to time, and with respect to V band magnitude are plotted in the bottom and top panels of Fig. 6, respectively. It is clearly seen that there are large variations in the spectral index between  $\sim 1.5$  to  $\sim 3.2$ . From Fig. 6 (bottom panel) it is clear that spectral index systematically increased with respect to time, and from Fig. 6 (top panel), the spectral index increases with respect to increasing V band magnitude, confirming the BWB result. The straight line fitting parameters are given in Table 7.

To understand the dominant emission mechanism in blazars, study of their spectral energy distribution (SEDs) is an important tool. Multi-wavelength SEDs can put constraints on physical parameters such as magnetic field, Doppler factor, jet power, etc. (Kushwaha et al. 2018a; Kushwaha, Sahayanathan, & Singh 2013). However, SEDs restricted to the optical band can still be used to understand some of a blazar's features and in particular, can look for the presence of new features, e.g. blue bumps (e.g. Kushwaha et al. 2018a). To examine this we have taken quasi-simultaneous B, V, R, and I band data points at four different states to produce optical SEDs. These states are: during outburst 1 from JD 2457756.5 – 2457757.5; during outburst 2 from JD 2457811.2 – 2457812.5; an intermediate state from JD 2457844.5 – 2457845.5; and a low state from JD 2457864.5 – 2457866.5. Unfortunately we only have data in two bands (V and R) at the lowest

**Table 7.** Spectral index variation with respect to JD and V band magnitude for entire period of observation campaign of OJ 287.

Parameter	$m_3^a$	$c_3^a$	$r_3^a$	$p_3^a$
$\alpha_{VR}$ vs JD	1.612E-03	-10.350	0.634	1.013E-14
$\alpha_{VR}$ vs V (mag)	3.054E-01	-2.123	0.650	1.235E-15

<sup>a</sup>  $m_3$  = slope and  $c_3$  = intercept of  $\alpha$  against JD or V;  
 $r_3$  = Pearson coefficient;  $p_3$  = null hypothesis probability

flux state of the source on JD 2458074 during this observing campaign and so could not plot an optical SED for it. To generate the SEDs, calibrated magnitudes of OJ 287 in B, V, R, I bands are adjusted for Galactic absorption, with  $A_B = 0.102$  mag,  $A_V = 0.077$  mag,  $A_R = 0.061$  mag, and  $A_I = 0.042$  mag, respectively (Cardelli, Clayton, & Mathis 1989; Bessell, Castelli, & Plez 1998). The SEDs of these four different flux states of the source are plotted in Fig. 7. During the observing campaign there were other periods of strong flaring as well as intermediate or low flux states of the source, but unfortunately we do not have quasi-simultaneous (within a day) observations in at least three optical bands, so those are not considered for making SEDs. A blue bump is seen on all SEDs which might be due to the thermal emission from the accretion-disc by the secondary black hole (e.g., Agarwal et al. 2015, 2016; Valtonen et al. 2016; Gupta et al. 2017a). Another possibility for this excess is that it might arise from broad line region (BLR) in the rest wavelength range  $\sim 200 - 400$  nm (Raiteri et al. 2007).

We have also plotted the spectral index following equation 4 with respect to V band magnitude in Fig. 8 for the four different flux states for which we have SEDs in Fig. 7. The modest variation of spectral indices with flux suggests that either the flares result from an increase in non-thermal particle density and/or that the bands have dominant contributions from other slowly (or not-highly variable) components, e.g. emission lines (e.g. Kushwaha et al. 2018a).

#### 4 DISCUSSION

In an extensive optical photometric and polarimetric monitoring campaign of the blazar OJ 287 on  $\sim 175$  nights during September 2016 – December 2017 that used nine optical telescopes around the globe, we searched for flux and colour variations on IDV, STV and LTV timescales. We also searched for colour variations with respect to time, colour dependence on magnitude, spectral index variation, SED changes, and polarization variations on LTV timescales. In 11 nights of quasi-simultaneous multi-band (V, R, I) observations, no genuine IDV in flux was detected which is also reflected in the lack of colour variations on IDV timescales. Strong evidence of flux and colour variations, including multiple instances of flaring, is noticed on STV and LTV timescales, and there is evidence for a BWB trend. OJ 287 showed large changes in the degree of polarization, and also large swings in polarization angle. The Stokes parameters changes show a systematic clockwise trend during the first hundred days, followed by an erratic variation and finally a return to a systematic trend. The optical spectral index varied between  $\sim 1.5 - 3.2$  and optical SEDs in the outburst states, an intermediate state, and the low flux state all show evidence of a blue bump.

Blazar flux variability on IDV timescales is the most puzzling, and during low states may allow us to probe very close to the central SMBH. IDV in high flux states can be due to evolution of the

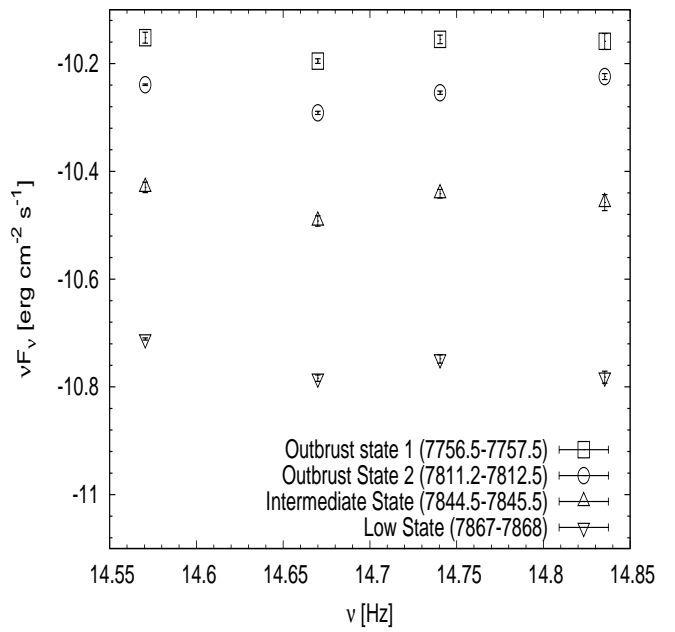


**Figure 7.** Optical spectral energy distribution (SED) of OJ 287 at different flux state.

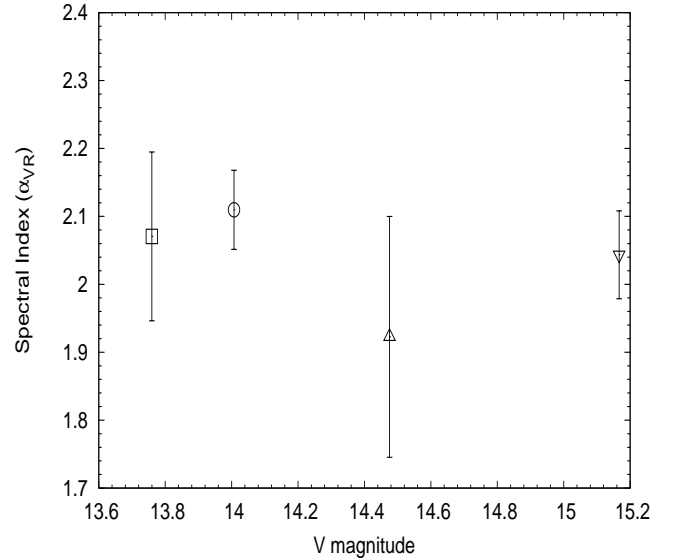


**Figure 8.** Variation of optical spectral index of OJ 287 with V magnitude during two outburst states, an intermediate state, and a low state, where the symbols have the same meaning as in Fig. 7.

electron energy density distribution of the relativistic charged particles in which shocks will accelerate relativistic particles in turbulent regions of plasma jets which then cool and lead to a variable synchrotron emission (Marscher, Gear, & Travis 1992; Marscher 2014; Calafut & Wiita 2015; O’Riordan et al. 2017). The most extreme IDV might require acceleration of small regions within the jets to extremely high Lorentz factors (e.g. Giannios et al. 2009). Optical flux variability detected on IDV timescales in low-states can be explained by models based on the accretion disc (e.g.,

([Mangalam & Wiita 1993](#); [Chakrabarti & Wiita 1993](#)). Our lack of detection of genuine IDV in any of the 11 densely sampled nights for OJ 287 indicates that during this period the jet emission was quite uniform and that relativistic shock directions did not quickly change with respect to our line of sight. Here we can safely rule out accretion disc based models because source was observed in an overall high flux state, when jet emission must dominate and no flux or colour variations were noticed on IDV timescales.

Blazar emission on STV and LTV timescales are dominated by non-thermal jet emission throughout the EM spectrum and can also explain the optical flux and polarization variability on diverse timescales. Shock-in-jet models (e.g. [Hughes, Aller, & Aller 1985](#); [Marscher & Gear 1985](#); [Spada et al. 2001](#); [Graff et al. 2008](#); [Joshi & Böttcher 2011](#), and references therein) can explain the general behaviour of flux variability on diverse timescales, while the polarization variability also can be explained by these models (e.g. [Marscher et al. 2008](#); [Larionov et al. 2013](#), and the references therein) particularly when supplemented with turbulence ([Marscher 2014](#)). Changes in the physical parameters set up close to the base of the jet including velocity, electron density, magnetic field, etc., can produce a new shock which can lead to a flaring event when moving along the inhomogeneous relativistic jet. Geometrical effects from jet bending, precession or internal helical structures can lead to changes in the Doppler boosting of the jet emission which can produce variety of flux variation on STV and LTV timescales in blazars (e.g. [Camenzind & Krockenberger 1992](#); [Gopal-Krishna & Wiita 1992](#); [Pollack, Pauls, & Wiita 2016](#)).

The four optical-IR SEDs (Fig. 7) during different flux states are almost flat, except for changes in the overall level of emission and a hint of blue bumps. In fact, it suggests more emission at the high frequency end, which is very different compared to previous SEDs ([Kushwaha et al. 2018a](#); [Gupta et al. 2017a](#); [Kushwaha, Sahayanathan, & Singh 2013](#)) where normally declining emission is seen, despite the presence of the blue bump feature. Since the blue bump does not vary appreciably on timescales of day-month, the flatness of the SED and the level of blue bump emission as was seen during our previous work ([Gupta et al. 2017a](#), see also [Kushwaha et al. \(2018a\)](#)) suggest contribution from another component in the optical that makes the emission increase at high frequencies (e.g. [Kushwaha et al. 2018b](#)). In fact, the high PD and strong changes during the observation, often associated with PA swings and the systematic variation in the fractional polarization suggest the new component to be non-thermal in nature, as also reflected in the strong variability of the optical V-R spectral index on daily timescales (Fig. 6).

In our flux and polarization monitoring campaign of OJ 287 during 2016 – 2017, we noticed interesting relations between the fluxes, degree of polarization, and polarization angle. There is a systematic swing of  $\sim 150^\circ$  in polarization angle from  $\sim$  JD 2457630 – JD 2457850, with a few superimposed short term fluctuations of up to  $\sim 50^\circ$ . But during this period the degree of polarization has large variations, (from a few percent to over 20 percent) sometimes correlated with the flux variation and sometimes anti-correlated with flux variation. Such changes in flux, degree of polarization, and polarization angle are quite complex. Interestingly the fractional polarization shows a systematic clockwise variation during the first 100 days, followed by an essentially random trend and again returning to systematic variation towards the end. It should be noted that the lack of observations before MJD  $\sim$  57650, allow an ambiguity of  $\pm 180^\circ$  in representation of PA. In our presentation of PA light curve here, we chose a smooth variation over a big jump, which differs by  $180^\circ$  to the presentation of some sim-

ilar data ([Valtonen et al. \(2017\)](#)). The choice is based on the fact the PD variation seen here is almost always associated with PA change and the fact that the fractional polarization shows both systematic and chaotic trends. Further, in random variation models, a sudden jump of no more than  $\pm 90^\circ$  is expected (e.g. [Marscher 2014](#)).

In the basic shock-in-jet model, where the shocked region strengthens the ordering of the magnetic field, one can expect a positive correlation between flux and polarization, i.e., an increase in polarization with an increase in flux ([Marscher & Gear 1985](#); [Marscher 1996](#); [Hagen-Thorn et al. 2008](#)). There are several cases in which blazar flux and degree of polarization show such positive correlations (e.g. [Larionov et al. 2008, 2013, 2016](#), and references therein) Detection of anti-correlated flux and degree of polarization is rare but has been occasionally noticed before (e.g. [Gaur et al. 2014](#)). During this observing campaign, we noticed that when the source goes into the lowest flux state  $\sim$  JD 2457865, the polarization fraction is rather high and there is evidence of large swings  $\sim 70^\circ$  of the polarization angle. ([Marscher et al. \(2008\)](#) gave a generalized model for variation in optical flux, degree of polarization, and polarization angle. The model involves a shock wave leaving the close vicinity of the central SMBH and propagating down only a portion of the jet's cross section which leads to the disturbance following a spiral path in a jet that is accelerating and becoming more collimated. [Larionov et al. \(2013\)](#) extended the work of ([Marscher et al. 2008](#)) and applied this generalized model to multiwavelength variations of an outburst detected in the blazar S5 0716+714. In the model of [Larionov et al. \(2013\)](#), if we change the bulk Lorentz factor  $\Gamma$ , even if the remaining parameters (e.g. jet viewing angle, temporal evolution of the outburst, shocked plasma compression ratio  $k$ , spectral index  $\alpha$ , and pitch angle of the spiral motion) are kept constant, different combinations in the variations in flux, polarization, and polarization angle can be observed.

## 5 SUMMARY

We summarized below our results:

- The blazar OJ 287 was in fairly bright state between September 2016 and December 2017 and several large and small flares were observed.
- Using our selection criteria, we had eleven nights during which multi-band intra-day LCs could be extracted but we never saw fast variations in flux or colour.
- On longer STV and LTV timescales OJ 287 showed large amplitude flux variation in all B, V, R, and I bands.
- Strong colour variations is noticed on STV and LTV timescales in both colour vs time and colour vs magnitude plots. A bluer-when-brighter trend was noticed between the V and R bands.
- There are strong variations in degree of polarization and large swings in polarization angle. For most of the occasions, flux and polarization variations are correlated.
- On one occasion, we noticed that there is strong evidence of anti-correlation in flux with degree of polarization and polarization angle.
- Through plotting the Stokes parameters, we observed that the fractional polarization exhibited a systematic clockwise trend with time during the first hundred days, followed by a more restricted and essentially random variation, and then it appears to revert to a systematic variation.

## ACKNOWLEDGMENTS

Data from the Steward Observatory spectropolarimetric monitoring project were used. This program is supported by Fermi Guest Investigator grants NNX08AW56G, NNX09AU10G, NNX12AO93G, and NNX15AU81G.

The work of ACG and AP are partially supported by Indo-Poland project No. DST/INT/POL/P19/2016 funded by Department of Science and Technology (DST), Government of India. ACG's work is also partially supported by Chinese Academy of Sciences (CAS) President's International Fellowship Initiative (PIFI) grant no. 2016VMB073. HG is sponsored by a CAS Visiting Fellowship for researchers from developing countries, CAS PIFI (grant no. 2014FFJB0005), supported by the NSFC Research Fund for International Young Scientists (grant no. 11450110398) and supported by a Special Financial Grant from the China Postdoctoral Science Foundation (grant no. 2016T90393). PJW is grateful for hospitality at KIPAC, Stanford University, and SHAO during a sabbatical. PK acknowledges support from FAPESP grant no. 2015/13933-0. The Abastumani team acknowledges financial support by the Shota Rustaveli National Science Foundation under contract FR/217950/16. OMK acknowledges China NSF grants NSFC11733001 and NSFCU1531245. SMHs work is supported by the National Natural Science Foundation of China under grants Nos. 11203016 and 11143012, Natural Science Foundation of Shandong province (No. JQ201702), and also partly supported by Young Scholars Program of Shandong University, Weihai. The work of ES, AS, RB was partially supported by the Bulgarian National Science Fund of the Ministry of Education and Science under the grants DN 08-1/2016 and DN 18-13/2017. GD and OV gratefully acknowledge the observing grant support from the Institute of Astronomy and NAO Rozhen, BAS, via bilateral joint research project "Study of ICRF radio-sources and fast variable astronomical objects" (the head is GD). This work is a part of the Projects no. 176011 "Dynamics and kinematics of celestial bodies and systems", no. 176004 "Stellar physics" and no. 176021 "Visible and invisible matter in nearby galaxies: theory and observations" supported by the Ministry of Education, Science and Technological Development of the Republic of Serbia. MFG is supported by the National Science Foundation of China (grants 11473054 and U1531245). ZZ is thankful for support from the CAS Hundred-Talented program (Y787081009).

## REFERENCES

- Agarwal A., Gupta A. C., 2015, MNRAS, 450, 541
- Agarwal A., et al., 2015, MNRAS, 451, 3882
- Agarwal A., et al., 2016, MNRAS, 455, 680
- Andruchow I., Cellone S. A., Romero G. E., Dominici T. P., Abraham Z., 2003, A&A, 409, 857
- Andruchow I., Combi J. A., Muñoz-Arjonilla A. J., Romero G. E., Cellone S. A., Martí J., 2011, A&A, 531, A38
- Bessell M. S., Castelli F., Plez B., 1998, A&A, 333, 231
- Blandford R. D., Rees M. J., 1978, Phys, 17, 265
- Calafut V., Wiita P. J., 2015, JApA, 36, 255
- Camenzind M., Krockenberger M., 1992, A&A, 255, 59
- Cardelli J. A., Clayton G. C., Mathis J. S., 1989, ApJ, 345, 245
- Cellone S. A., Romero G. E., Combi J. A., Martí J., 2007, MNRAS, 381, L60
- Chakrabarti S. K., Wiita P. J., 1993, ApJ, 411, 602
- de Diego J. A., 2010, AJ, 139, 1269
- Fiorucci M., Tosti G., 1996, A&AS, 116, 403
- Gaur H., Gupta A. C., Lachowicz P., Wiita P. J., 2010, ApJ, 718, 279
- Gaur H., Gupta A. C., Wiita P. J., 2012a, AJ, 143, 23
- Gaur H., et al., 2012b, MNRAS, 420, 3147
- Gaur H., et al., 2012c, MNRAS, 425, 3002
- Gaur H., Gupta A. C., Wiita P. J., Uemura M., Itoh R., Sasada M., 2014, ApJ, 781, L4
- Gaur H., et al., 2015, MNRAS, 452, 4263
- Ghisellini G., et al., 1997, A&A, 327, 61
- Giannios D., Uzdensky D. A., Begelman M. C., 2009, MNRAS, 395, L29
- Gopal-Krishna, Wiita P. J., 1992, A&A, 259, 109
- Gopal-Krishna, Stalin C. S., Sagar R., Wiita P. J., 2003, ApJ, 586, L25
- Goyal A., Gopal-Krishna, Wiita P. J., Anupama G. C., Sahu D. K., Sagar R., Joshi S., 2012, A&A, 544, A37
- Graff P. B., Georganopoulos M., Perlman E. S., Kazanas D., 2008, ApJ, 689, 68
- Gu M. F., Lee C.-U., Pak S., Yim H. S., Fletcher A. B., 2006, A&A, 450, 39
- Gupta A. C., Banerjee D. P. K., Ashok N. M., Joshi U. C., 2004, A&A, 422, 505
- Gupta A. C., Fan J. H., Bai J. M., Wagner S. J., 2008, AJ, 135, 1384
- Gupta A. C., et al., 2012, MNRAS, 425, 1357
- Gupta A. C., et al., 2016, MNRAS, 458, 1127
- Gupta A. C., et al., 2017a, MNRAS, 465, 4423
- Gupta A. C., et al., 2017b, MNRAS, 472, 788
- Hagen-Thorn V. A., Larionov V. M., Jorstad S. G., Arkharov A. A., Hagen-Thorn E. I., Efimova N. V., Larionova L. V., Marscher A. P., 2008, ApJ, 672, 40
- Heidt J., Wagner S. J., 1996, A&A, 305, 42
- Hu S.-M., Han S.-H., Guo D.-F., Du J.-J., 2014, RAA, 14, 719
- Hughes P. A., Aller H. D., Aller M. F., 1985, ApJ, 298, 301
- Joshi M., Böttcher M., 2011, ApJ, 727, 21
- Kirk J. G., Rieger F. M., Mastichiadis A., 1998, A&A, 333, 452
- Kushwaha P., Sahayanathan S., Singh K. P., 2013, MNRAS, 433, 2380
- Kushwaha P., et al., 2018b, In preparation
- Kushwaha P., et al., 2018, MNRAS, 473, 1145
- Larionov V. M., et al., 2008, A&A, 492, 389
- Larionov V. M., et al., 2013, ApJ, 768, 40
- Larionov V. M., et al., 2016a, MNRAS, 461, 3047
- Lehto H. J., Valtonen M. J., 1996, ApJ, 460, 207
- Mangalam A. V., Wiita P. J., 1993, ApJ, 406, 420
- Marcha M. J. M., Browne I. W. A., Impey C. D., Smith P. S., 1996, MNRAS, 281, 425
- Marscher A. P., Gear W. K., 1985, ApJ, 298, 114
- Marscher A. P., 1996, in ASP Conf. Series, 110, Blazar Continuum Variability, ed. H. R. Miller, J. R. Webb, & J. C. Noble (San Francisco, CA: ASP), 248
- Marscher A. P., Gear W. K., Travis J. P., 1992, Variability of Blazars, Cambridge Univ. Press, Cambridge, p. 85
- Marscher A. P., et al., 2008, Natur, 452, 966
- Marscher A. P., 2014, ApJ, 780, 87
- Miller H. R., Carini M. T., Goodrich B. D., 1989, Natur, 337, 627
- Moore R. L., et al., 1982, ApJ, 260, 415
- O'Riordan M., Pe'er A., McKinney J. C., 2017, ApJ, 843, 81
- Pollack M., Pauls D., Wiita P. J., 2016, ApJ, 820, 12
- Raiteri C. M., et al., 2007, A&A, 473, 819
- Schlafly E. F., Finkbeiner D. P., 2011, ApJ, 737, 103
- Sillanpää A., Haarala S., Valtonen M. J., Sundelius B., Byrd G. G., 1988, ApJ, 325, 628
- Sillanpää A., et al., 1996a, A&A, 305, L17
- Sillanpää A., et al., 1996b, A&A, 315, L13
- Smith P. S., Montiel E., Rightley S., Turner J., Schmidt G. D., Jannuzzi B. T., 2009, arXiv, arXiv:0912.3621
- Spada M., Ghisellini G., Lazzati D., Celotti A., 2001, MNRAS, 325, 1559
- Stalin C. S., Gopal Krishna, Sagar R., Wiita P. J., 2004, JApA, 25, 1
- Stocke J. T., Morris S. L., Gioia I. M., Maccacaro T., Schild R., Wolter A., Fleming T. A., Henry J. P., 1991, ApJS, 76, 813
- Urry C. M., Padovani P., 1995, PASP, 107, 803
- Valtonen M. J., et al., 2008a, Natur, 452, 851
- Valtonen M., Kidger M., Lehto H., Poyner G., 2008b, A&A, 477, 407

- Valtonen M. J., et al., 2009, *ApJ*, 698, 781  
Valtonen M. J., et al., 2010, *ApJ*, 709, 725  
Valtonen M. J., et al., 2016, *ApJ*, 819, L37  
Valtonen M., et al., 2017, *Galax*, 5, 83  
Wagner S. J., Witzel A., 1995, *ARA&A*, 33, 163  
Wiercholska A., Ostrowski M., Stawarz Ł., Wagner S., Hauser M., 2015,  
A&A, 573, AA69  
Woo J.-H., Urry C. M., 2002, *ApJ*, 579, 530